Progress in Reaction Kinetics and Mechanism

ARTICLE

Open Access

https://doi.org/10.48130/prkm-0025-0009

Progress in Reaction Kinetics and Mechanism **2025**, 50: e009

Application of charged micelle generators on the oxidation of metabisulphite ion by molybdenum-oxime complex: Piszkiewicz kinetic model

Ikechukwu Ugbaga Nkole[1*], Sulaiman Ola Idris[2], Ibrahim Abdulkadir[2] and Ameh David Onu[3]

[1] *Basic Science Unit, Wigwe University, Isiokpo, Rivers State, 811101, Nigeria*
[2] *Department of Chemistry, Ahmadu Bello University, Zaria, 810107, Nigeria*
[3] *Department of Chemistry, Federal University of Education, Zaria, 810282, Nigeria*
* Corresponding author, E-mail: ikechukwu.ugbaga@wigweuniversity.edu.ng

Abstract

The chemical characteristics of sulfur oxyanions as antioxidants is an interesting course worth probing, and understanding their mechanistic pathway is key. Hence, the application of charged micelle generators on the oxidation of the metabisulphite ion by the molybdenum-oxime complex (MOC) is suggested. Piszkiewicz's model is checked, and its dynamics are explored to offer explanations on the implication of the surfactants' involvement in the redox behavior of metabisulphite with the MOC. The reaction reveals a strong dependence of reaction rate on the positively charged micelles of cetyltrimethylammonium bromide (CTAB) compared to the negatively charged micelles of sodium dodecyl sulfate (SDS) due to the high cooperativity order exhibited by the CTAB with the substrates, which are supported by a remarkable binding constant that exists between them within the Palisade-Stern layer region of the micelle. The inhibitory results exerted by SDS on the reaction rate infers a probable repulsion between it and the reactant at the head polar layer of the micelle. The influence of cationic (NH_4^+) and anionic ($HCOO^-$) counter-ions on the oxidation rate supplements the role of the surfactant's interaction with the redox partners at the slow phase. The contribution of ion concentration to the oxidation rate depicts a reaction proceeding through a positive Brønsted salt effect, and the variation in the oxidation-environment polarity strengthened the outcome of the varied ion concentration on the oxidation rate, which is clarified better by Piszkiewicz's model. Sulfur oxyanion radical was imperative in the reduction route of the coordinated MOC by the metabisulphite ion.

Citation: Nkole IU, Idris SO, Abdulkadir I, Onu AD. 2025. Application of charged micelle generators on the oxidation of metabisulphite ion by molybdenum-oxime complex: Piszkiewicz kinetic model. *Progress in Reaction Kinetics and Mechanism* 50: e009 https://doi.org/10.48130/prkm-0025-0009

Introduction

The metabisulphite ion is a chemically reactive nucleophile that acts as an inhibitor of microbial development, food spoilage, color enhancement, enzymatic activities, and oxidative processes in biological systems[1–5]. It has a high probability of affecting the nutritive value of food by interacting with folic acid, thiamine, nicotinamide, and pyridoxal vitamins found in it, hence stimulating its degradation[6]. Baker et al.[7] reported that sulfite from the metabisulphite preservative in the 2,6-diisopropyl phenol (propofol) blend generates an oxidative medium when this blending is opened to air, leading to the dimerization and decolorization of the product, which was attributed to the swift development of the reactive sulfite radical. The study of the possible toxic effects of $Na_2S_2O_5$ on human foreskin cells *in vitro* revealed that there was a reduction in cell viability on varying the concentration of the antioxidant and an increment in the reactive oxygen species levels in the treated cells. Indicative of significant exertion of toxic effects on human cells via several mechanistic routes such as atom transfer, electron transfer, atom and electron transfer, free radicals facilitated, and intermediates promoters' routes by the sodium metabisulphite[8].

Zohra et al.[9] documented the consequence of subchronic incorporation of $Na_2S_2O_5$ on lipid peroxidation, protein, and enzymatic antioxidants in the gastric tissue and splenic Wister rat. It was observed that the subchronic intake of $Na_2S_2O_5$ had a hostile consequence on the spleen and stomach by initiating oxidative impairment, leading to an acceleration in lipid peroxidation and an adjustment of enzymatic activity. The effect of a 28-amino acid acylated peptide esterified with octanoic acid on Ser 3 (Ghrelin) given to the Wister rat on sulfite initiated oxidative and apoptotic change in its intestinal mucosa, resulting in a notable decrease in intestinal total oxidant status. The sodium metabisulphite initiated a notable rise in the total oxidant status and number of apoptotic cells. The action of Ghrelin in the process reduced the number of apoptotic cells[10]. The influence of $Na_2S_2O_5$ as an antioxidant in overwhelming the drug release change from aged polyox tablets was reported. It was observed that the presence of $Na_2S_2O_5$ steadied the release of the drug from polyethylene oxide (PEO) matrices, and the absence of it caused a surge in drug release from polyox matrices when stored at 40 °C. Thus, the concentrations of $Na_2S_2O_5$ investigated were able to restrain the structural alterations of polyox samples and steadied the drug release[11]. Because food additives are liable to initiate allergic reactions that implicate an immune mechanism, there is a need to have a detailed understanding of their redox behavior and mechanistic routes in a regulated medium.

In addition, a molybdenum framework with bismuth has been explored as a catalyst in the photo-degradation process of methylene blue dye (MBD), as convened by Alahmadi et al.[12]. The team asserted that the Bi-Mo nano-framework (Bi_2O_3/$MoSe_2$) enhanced the MBD degradation more than the individual species (Bi_2O_3 and $MoSe_2$) due to its improved surface area and crystallinity, which is characterized by smaller particle size.

The study of the effect of charged micelle generators on a reaction medium is key to understanding the realities of solvent effect on the rate of reactions. The micelle media are sustainable, recoverable, and have a direct drive on reaction rate, and they position surfactants as a more reliable medium than organic solvents might take part in the reaction by oxidizing or reducing themselves[13–15]. CTAB and SDS with cationic and anionic polar heads respectively, have demonstrated useful interaction/binding traits with substrates.

Quantitatively, their influence on the reaction rate has been determined using Piszkiewicz's, Berezin's, and Pseudophase ion-exchange models. The models presume the distribution of the substrates over the whole bulk of the micelles[16–18]. However, Srivastava and coworkers[19] pointed out the non-supportive character of CTAB and SDS in the oxidation of acid-red-13 dye with peroxydisulphate and neutrality of triton X-100 on the catalysis of the dye degradation process was obvious. In the oxidation system of l-phenylalanine with chromic acid, triton X-100, and SDS facilitated the oxidation process, whereas CTAB dragged the reaction rate due to the charge state of the substrates at the slow step[20]. In the same vein, CTAB elevated the oxidation of l-phenylalanine with Fe(III)-cyano complex, which was attributed to hydrophilic supremacy[21]. In a system where opposite charge species dominate such as oxidation of l-leucine with Fe(III)-cyano complex, CTAB also adequately accelerated the process and SDS championed an opposite influence[22]. A similar observation was reported in the oxidation of L-glutamic acid with the complex[23]. On the other hand, The analogue of CTAB, cetylpyridinium chloride was employed to accelerate the oxidation of l-phenylalanine with Cu(III)-periodate complex and the impact was massive with four-fold increment in reaction rate compared to surfactant-free system[24]. The same analogue of CTAB replicated the influence on the oxidation of l-glutamic acid with Fe(III)-cyano complex and impediment was noticed at high concentrations of the surfactant due to ion saturation[25].

The impact of molybdenum, as a constituent of nitrogenase enzymes, on the oxidation of nitrogen to ammonium during nitrogen fixation in plants, and the alteration of ruminant animal skin color when it is in excess holds promise for a better understanding of its redox mechanistic route[26]. Hence, a need to have detailed information on the mechanistic pathway of their electron transfer reaction and quantitatively determine the micelle-substrates hydrophobic and hydrophilic effects.

Experimental

Materials

Sigma Aldrich, Germany: syn-2-pyridinealdoxime (99% pure), cetyltrimethylammonium bromide (99% pure), molybdenum(IV) oxide (99.9 % pure), and sodium dodecyl sulfate (99% pure) were used. $Na_2S_2O_5$ (97% pure), HCl (37% pure), NH_4Cl (99.5% pure), HCOONa (98% pure), $SnCl_2$ (97% pure), $K_2Cr_2O_7$ (99.5% pure), $BaCl_2$ (99% pure), H_2SO_4 (98% pure), KSCN (98% pure), NaCl (99.9% pure), ethanol (95% pure), methanol (99.5% pure), acrylamide (98.5% pure), sodium ascorbate (98% pure), sodium nitroprusside (98% pure), and diethyl ether (99% pure) were purchased from Fisher Chemical (Nigeria).

Synthesis of molybdenum-oxime complex

The approach by Konidaris et al.[27] was engaged in the synthesis of the MOC and the synthetic detail is recorded in our previous work on the redox reaction of allylthiourea with MOC[18], and it was characterized with an FTIR Spectrometer (Model-8400S, Shimadzu), UV spectrometer (Cary 300 Series), and conductivity meter (HACH Sension5).

Rate measurement

The reactant's mole contribution was learned as described beforehand[28–30] using photo-titrimetric at a constant electrolyte concentration and temperature. The point of interpolation on the display of absorbance against mole proportionality signaled the reaction stoichiometry.

A 721 PEC Medical ultraviolet-spectrometer model was involved in the kinetic surveys by noting the drop in concentration using change in absorbance of the molybdenum-oxime complex following the pseudo-first-order protocol with $[S_2O_5^{2-}]$ in a ten-fold multiple over the [MOC][31–38]. The adjustment in the salt concentration (μ), medium polarity (D), and the $[H^+]$ involvement in the oxidation was probed by varying one at a time while upholding the other parameters at a fixed amount[39–42]. The observed rate constant (k_{ob}) was assessed from the slope of the relationship between InA vs t [Eqn (1)], and the rate constant (k_2) was secured from the segmentation of k_{ob} with $[S_2O_5^{2-}]$ [Eqn (2)]. Discovery of free radicals was made possible by the inclusion of acrylamide solution (0.15 cm^3) and methanol (5 cm^3) in the reaction in progress[43–46].

$$\mathrm{InA} = \mathrm{InA}_0 + k_{ob}t \quad (1)$$

$$k_2 = k_{ob}/[S_2O_5^{2-}] \quad (2)$$

Micelle formation and kinetic model

Micelle formation was verified via the critical micelle concentration, CMC, of the surfactants, which was obtained by measuring the specific conductivities of various [surfactant] solutions. The conductivity meter was attuned using 0.02 molar sodium chloride. The interjection point in the conductivity-concentration graph was considered as the CMC[47,48]. Piszkiewicz's model was explored following its scientific equation [Eqn (3)].

$$k_{ob} = \frac{k_w K_D + k_m [D]^n}{K_D + [D]^n} \quad (3)$$

Thus, K_D is the detachment constant of the micelle back to its free components. k_w and k_m are the reaction rate constants in the absence and presence of surfactant accordingly. n is the number of surfactant molecules (D) and k_{ob} is the pseudo-first-order rate constant. [D] is the surfactant concentration[14,49].

Results and discussion

Characterization of synthesized MOC

The UV/visible spectrophotometer of the MOC produced a maximum wavelength of 560 nm. The FTIR spectra of the oxime-ligand and the MOC are presented in Figs 1 and 2, respectively. The molecular vibrations of the MOC and ligand, and the conductivity measurement of the MOC are presented in Table 1.

The observed molar conductivity of 133 S $cm^2 \cdot mol^{-1}$ (Table 1), depicts the electrolytic nature of the MOC in solution[50–52].

The band observed at 3,075.1 cm^{-1} from the FTIR spectrum of the ligand (Fig. 1) is assigned to C-H stretching and 1,654.9 cm^{-1} band is assigned to C=N stretching, which shifted to 1,300.7 cm^{-1} in the MOC as a result of the C-N vibrational mode (Fig. 2). Indicative of complexation of the imine group with the central metal ion. The bands observed at 767.1 and 745.5 cm^{-1} in the spectrum of MOC are assigned to Mo=O stretching, indicating symmetrical and antisymmetrical vibrations of MoO_2 with a cis-MoO_2 orientation, as a trans-MoO_2 component would typically show one Mo=O band due to the asymmetry stretch, while that at 584.7 cm^{-1} is assigned to Mo-N stretching[53].

Stoichiometry

The resultant mole proportionality describes a two-electron contribution from a mole of the $S_2O_5^{2-}$ ion to the 2 moles of the MOC (Eqn. (4) as shown in Fig. 3). The place of interjection in Fig. 4 establishes the number of moles implicated in the reaction.

The involvement of an unequal mole of the reactants results in the realization of SO_4^{2-} ion, SO_2, and Mo^{2+} products, which are confirmed classically. The appearance of an insoluble white precipitate on the addition of $BaCl_2$ solution and in excess HCl confirms the

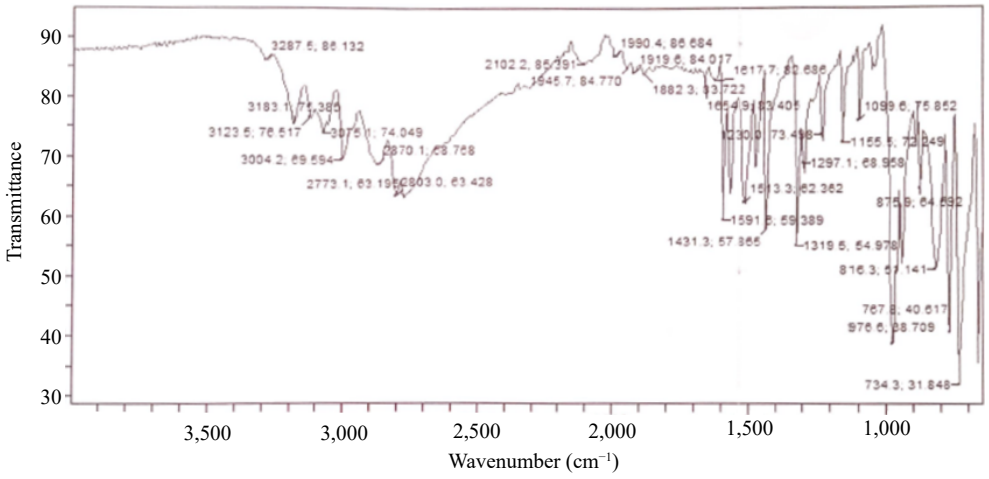

Fig. 1 Oxime-ligand FTIR spectrum.

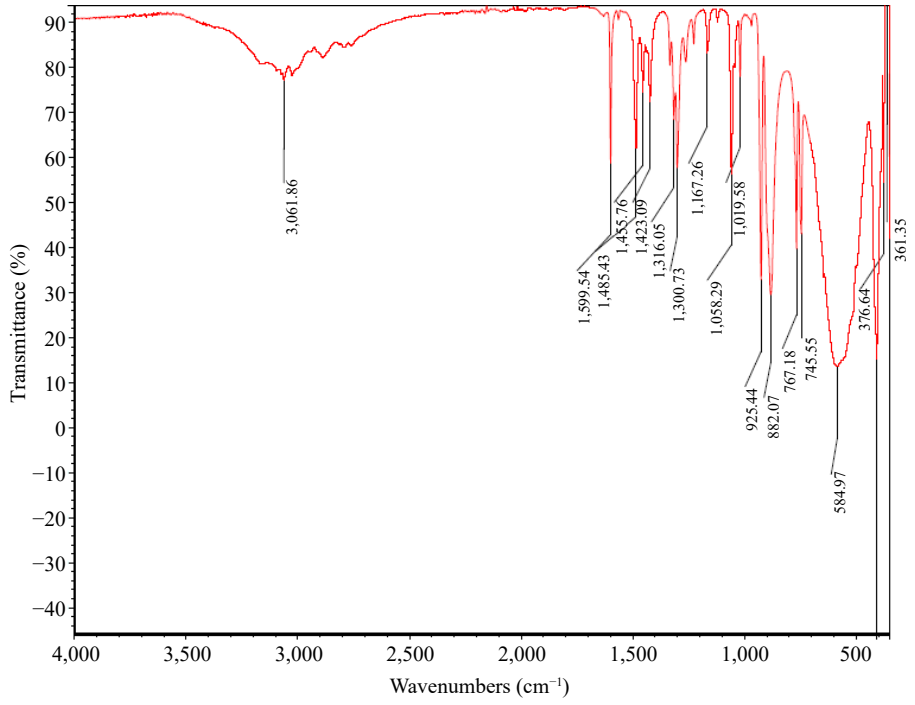

Fig. 2 MOC FTIR spectrum.

Table 1. Molecular vibrations of interest for the MOC and its molar conductivity.

Item	Band (cm^{-1})	Assignment
Ligand	1,654.9	C=N (stretching)
	1,591.8	N-O (bending)
MOC	767.1 & 745.5	Mo=O (stretching)
	584.7	Mo-N (stretching)
	1,300.7	C-N (stretching)
	1,599.5	N-O (bending)
Molar conductivity	133 $S{\cdot}cm^2{\cdot}mol^{-1}$	

presence of SO_4^{2-} ion[54]. The change of the damp filter paper dipped in acidified potassium dichromate from orange to green indicates the presence of SO_2[55]. The formation of a red color on the addition of three drops of KSCN solution (0.3 M) and two drops of acidified $SnCl_2$ solution (0.14 M) infers the manifestation of the Mo^{2+} ion product [Eqn (4) shown in Fig. 3][56].

Kinetic investigations

The probing of the observed rate constant, $k_{ob,}$ through the graph that relates absorbance with time (Fig. 5), the output discloses a straight path that authenticates an oxidation with a single-order in the MOC concentration. The incline (1.0019) of the curve of log k_{ob} against log $[S_2O_5^{2-}]$ (Fig. 6) also suggests a single-order in the $[S_2O_5^{2-}]$. Protonation of the $S_2O_5^{2-}$ ion [Eqn (5) shhown in Fig. 11] is accommodated in the process, which necessitated an increase in the rate of the reduction-oxidation process as the $[H^+]$ is amplified (Table 2). The redox-rate is accelerated as the electrolyte concentration in the system is adjusted, originating from the collision of identical-charged species at the slow step [Eqn (6) shhown in Fig. 11], and this is reinforced by the deceleration of the oxidation speed on the change in the reaction system dielectric constant from 77.2–71.2 with ethanol (Table 3). There is a manifestation of the association of similar charged moieties at the slow step when the oxidation of $S_2O_5^{2-}$ ion is catalyzed and inhibited by the inclusion of NH_4^+ and $HCOO^-$ ions, respectively (Table 4), standing as an indicator of an

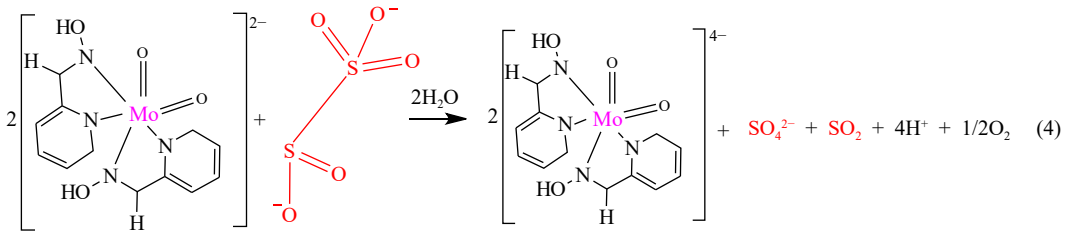

Fig. 3 Stoichiometric equation of the reaction of MOC and metabisulphite ion.

interaction involving an outer sphere mechanism. However, the generated sulfite radicals were essential in the formation of sulfur dioxide and reduction of the MOC [Eqn (7) shown in Fig. 11].

Relatively, the metabisulphite oxidation with hexacyanoferrate (III), HCF, in buffer system convenes inverse [H+] impact on the rate constant with the generation of hydrogen sulfite and sulfite radicals that recombined to form dithionate ions in a fast mode. Oxidation was favored by high solvation of active ion species, which made the outer coordination of HCF a center for interaction and implicated an outer-sphere mechanism, as supported by a large entropy of activation (−205 J·K−1·mol−1)[57].

Kinetically, the intermediate formation is confirmed by using a Lineweaver-Burk plot, a modification of Michaelis-Menten plot (Fig. 7), where lack of intercept is an indication of non-availability of intermediate species and vice versa. Thus, the structural integrity of the complex remains intact due to the stability emanating from the crystal field stabilization energy, the metal ion, and the strong field ligand at an average temperature.

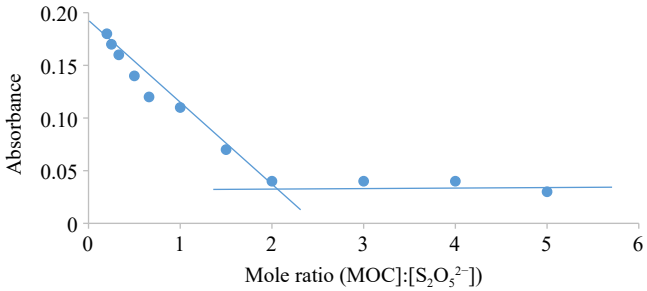

Fig. 4 Graph of Abs vs mole ratio for the oxidation of $S_2O_5^{2-}$ by MOC. Condition: [MOC] = 1.9 × 10^{-3} mol·dm^{-3}, [$S_2O_5^{2-}$] = (0.4.18 – 95.0) × 10^{-4} mol·dm^{-3}, [H^+] = 0.02 mol·dm^{-3}, T = 301 K, λ_{max} = 560 nm.

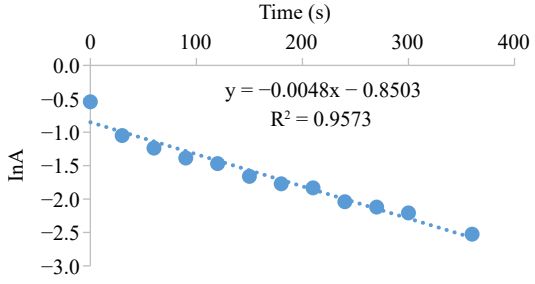

Fig. 5 Typical pseudo-first order plot for the oxidation of $S_2O_5^{2-}$ by MOC. Condition: [MOC] = 1.9 × 10^{-3} mol·dm^{-3}, [$S_2O_5^{2-}$] = 9.5 × 10^{-2} mol·dm^{-3}, [H^+] = 0.02 mol·dm^{-3}, T = 301 K, λ_{max} = 560 nm.

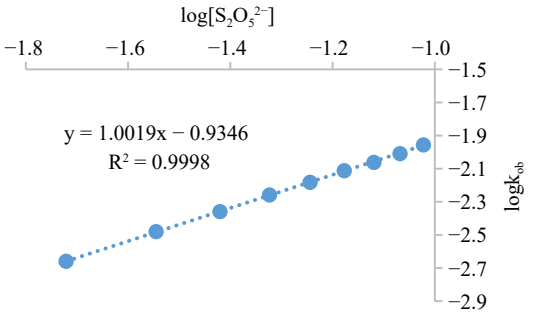

Fig. 6 Graph of $logk_{ob}$ against log[$S_2O_5^{2-}$] for the oxidation of $S_2O_5^{2-}$ by MOC. Condition: [MOC] = 1.9 × 10^{-3} mol·dm^{-3}, [$S_2O_5^{2-}$] = (1.9 – 11.4) × 10^{-2} mol·dm^{-3}, [H^+] = 0.02 mol·dm^{-3}, T = 301 K, λ_{max} = 560 nm.

Effect of micelle generators

The CTAB and SDS micelles generation in H_2O:ethanol mixture at 301 K is confirmed from the point of interjections (32.0 × 10^{-4} and 90.0 × 10^{-4} M, respectively) at the conductivity-concentration graphs (Figs 8 and 9), which depict the concentration at which surfactants aggregate to form micelles. Comparative investigation showed that in the presence of 0.1 M KNO_3, CMCs of 4.0 × 10^{-3} and

Table 2. Rate constants for the oxidation of $S_2O_5^{2-}$ ion by MOC.

$10^2[S_2O_5^{2-}]$ (mol·dm^{-3})	$10^2[H^+]$ (mol·dm^{-3})	μ (mol·dm^{-3})	10^3k_{ob} (s^{-1})	10^2k_2 (dm^3·mol^{-1}·s^{-1})
1.9	2.0	0.40	2.53	11.53
2.9	2.0	0.40	3.92	11.61
3.8	2.0	0.40	4.61	11.52
4.8	2.0	0.40	5.99	11.61
5.7	2.0	0.40	7.14	11.53
6.7	2.0	0.40	8.52	11.62
7.6	2.0	0.40	9.21	11.40
8.6	2.0	0.40	10.13	11.45
9.5	2.0	0.40	11.05	11.64
10.5	2.0	0.40	12.21	11.68
11.4	2.0	0.40	13.13	11.52
9.5	2.0	0.40	11.05	11.64
9.5	2.5	0.40	11.52	12.12
9.5	3.0	0.40	12.21	12.84
9.5	3.5	0.40	12.44	13.09
9.5	4.0	0.40	12.89	13.58
9.5	4.5	0.40	13.13	13.82
9.5	5.0	0.40	14.05	14.79
9.5	5.5	0.40	14.74	15.51
9.5	6.0	0.40	16.58	17.45
9.5	6.5	0.40	17.50	18.42
9.5	7.0	0.40	17.96	18.91
9.5	2.0	0.35	9.21	9.69
9.5	2.0	0.40	11.05	11.64
9.5	2.0	0.45	11.98	12.61
9.5	2.0	0.50	12.67	13.33
9.5	2.0	0.55	14.05	14.79
9.5	2.0	0.60	16.59	17.45
9.5	2.0	0.65	18.65	19.63
9.5	2.0	0.70	21.42	22.55
9.5	2.0	0.80	25.33	26.67
9.5	2.0	0.85	34.55	36.36

Condition: [MOC] = 1.9 × 10^{-3} mol·dm^{-3}, [H^+] = 0.02 mol·dm^{-3}, T = 301 K, λ_{max} = 560 nm.

Table 3. Effect of medium polarity on the oxidation speed of $S_2O_5^{2-}$ ion by MOC at λ_{max} = 560 nm.

D	10^3k_{ob} (s^{-1})	10^2k_2 ($dm^3{\cdot}mol^{-1}{\cdot}s^{-1}$)
77.2	11.05	11.64
76.5	9.44	9.94
75.9	9.21	9.69
75.2	7.83	8.24
74.5	7.14	7.52
73.9	6.45	6.79
73.2	5.53	5.82
72.5	4.61	4.85
71.9	4.38	4.61
71.2	3.92	4.12

Condition: [MOC] = 1.9 × 10^{-3} mol·dm^{-3}, [$S_2O_5^{2-}$] = 9.5 × 10^{-3} mol·dm^{-3}, [H^+] = 0.02 mol·dm^{-3}, T = 301 K, λ_{max} = 560 nm.

Table 4. Effect of counter-ions on the oxidation speed of $S_2O_5^{2-}$ ion by MOC at λ_{max} = 560 nm.

Ion	10^3[Ion] (mol·dm^3)	10^3k_{ob} (s^{-1})	10^2k_2 ($dm^3{\cdot}mol^{-1}{\cdot}s^{-1}$)
NH_4^+	0.00	11.05	11.64
	8.00	12.21	12.85
	12.0	12.46	13.43
	16.0	12.89	13.58
	20.0	13.36	14.06
	24.0	14.05	14.79
	28.0	11.95	15.76
$HCOO^-$	0.00	11.05	11.64
	8.00	9.90	10.42
	12.0	8.06	8.42
	16.0	7.37	7.76
	20.0	5.76	6.06
	24.0	5.07	5.33
	28.0	4.38	4.61

Condition: [MOC] = 1.9 × 10^{-3} mol·dm^3, [$S_2O_5^{2-}$] = 9.5 × 10^{-3} mol·dm^{-3}, [H^+] = 0.02 mol·dm^{-3}, T = 301 K, λ_{max} = 560 nm.

7.0 × 10^{-4} M were reported for SDS and CTAB, respectively. The presence of salt concentration in surfactant solutions was attributed to the decline in the CMCs[58]. Wei et al.[59] reported CTAB CMC of 9 × 10^{-4} and 0.24 M in water and ethanol, respectively at ambient temperature. Thus, CMC decreases by shrinking the repulsive action between the charged-head groups of the surfactant monomers and it works against micelle formation, making micelles form at a reduced surface-active agent concentration[36].

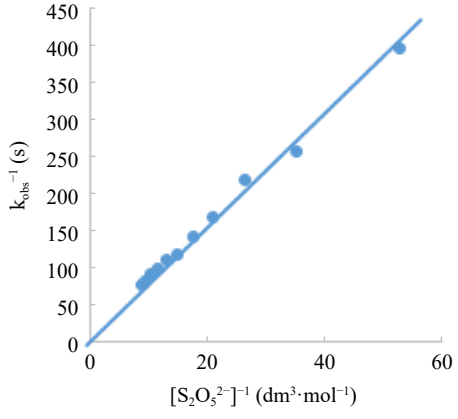

Fig. 7 Lineweaver-Burk plot of Michealis-Menten's plot modification for intermediate determination.

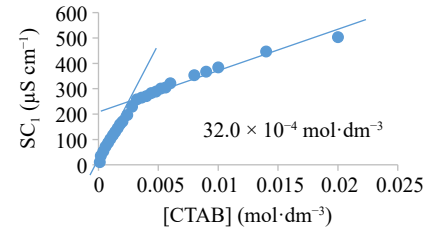

Fig. 8 Specific conductance-concentration curve for CTAB.

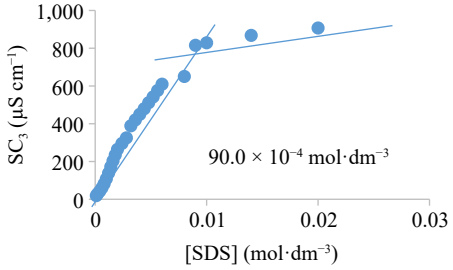

Fig. 9 Specific conductance-concentration curve for SDS.

The influence of cetyltrimethylammonium bromide on the oxidation rate of the $S_2O_5^{2-}$ ion by which the Piszkiewicz model is examined illuminates a substantial binding (K_D^{-1}) and cooperativity (n > 1) prevailing between the substrate and micelle, which results in an increased oxidation rate. This effect can be attributable to the associative mode that is assumed by the CTAB's polar head with the charged MOC on the Stern stratum of the CTAB aggregates, which is well-thought-out to possesses a great ionic concentration of the CTAB and reduced polarity. The catalytic micelle – substrate model of Piszkiewicz's concept based on enzymatic bimolecular oxidation of metabisulphite ion by MOC is presented in Fig. 10, wherein M^{2-} is the MOC, *Kn'* is the association constant of the extra interactions, and n' is the extra number of *CTAB* monomers. The undeviating minimum-squares style is employed in estimating the factors of Eqn (3) (Table 5).

Furthermore, the result of SDS on the oxidation speed of $S_2O_5^{2-}$ ion expresses weak ionic and non-ionic collaborations between the SDS and the $S_2O_5^{2-}$ - MOC at the Gouy-Chapman district of the micelle. This is perhaps connected to the association of similar charged moieties at the speed-limiting phase [Eqn (6) shown in Fig. 11], indicating that the $S_2O_5^{2-}$ - MOC moieties associated inade-

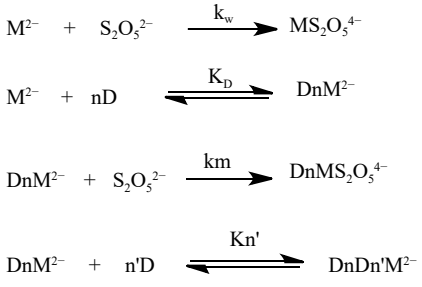

Fig. 10 The catalytic micelle - substrate model of Piszkiewicz's concept.

Table 5. Factors of Piszkiewicz kinetic model.

Micelle generator	n	K_D	K_D^{-1}	k_m ($dm^3{\cdot}mol^{-1}{\cdot}s^{-1}$)	r^2	k_w ($dm^3{\cdot}mol^{-1}{\cdot}s^{-1}$)
CTAB	1.4955	0.6114	1.6355	0.8623	0.9898	0.1164
SDS	2.2751	0.8367	1.1951	0.0155	0.9451	0.1164

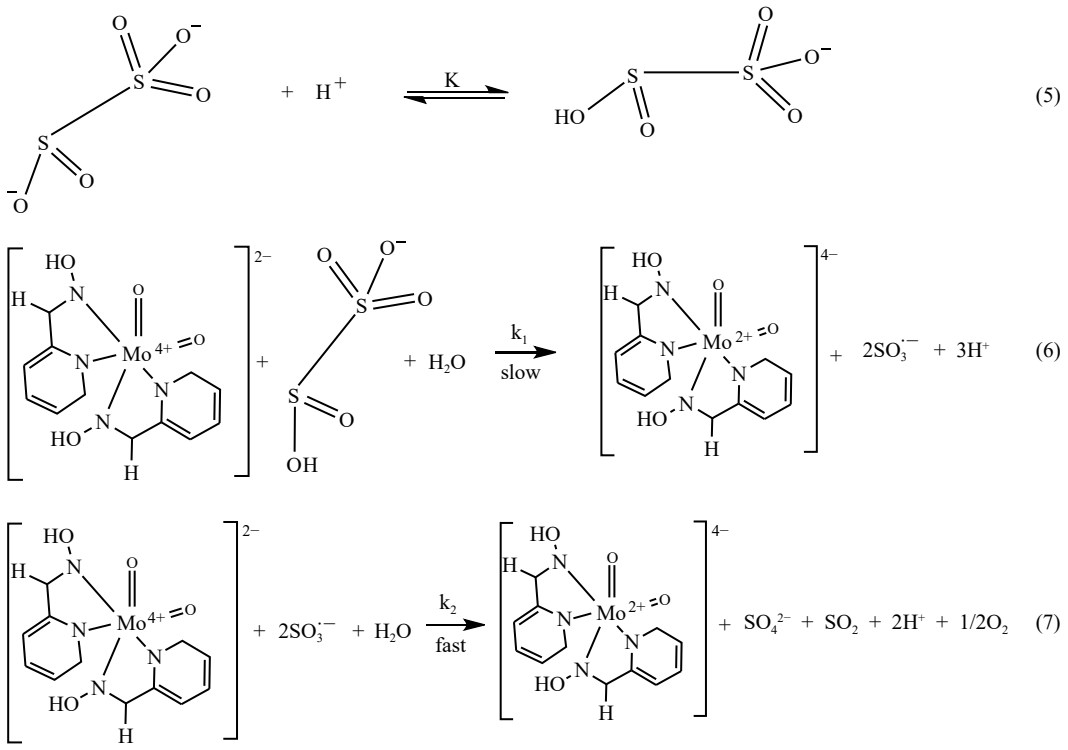

Fig. 11 Simple redox routes of MOC and $S_2O_5^{2-}$.

quately with the SDS aggregates that occasioned an unfavorable collision between them. The control of the inhibitory effect above the catalytic action of SDS on the oxidation rate is strengthened by a lower associative constant (1.1951) of the micelle with the substrates compared to the associative constant (1.6355) of the CTAB micelle with the substrate. The stratum of this interaction can be assumed to be a district of lower ionic concentration and lower aggregate separation. Thus, CTAB and SDS increase and decrease the rate by 7-fold and 8-fold, respectively, compared to aqueous: ethanol medium and the result recommends that Piszkiewicz's approach is pertinent in this redox route. The usage of the model gives substantial evaluation coefficients (r^2) and the k_m is higher than the corresponding k_w value, which marks the model as effective.

Owing to the above kinetic evidence, a mechanism without an intermediate is proposed [Eqns (5)–(7)] as offered in Fig. 11.

$$\text{Rate law} = k_1[\text{MOC}][HS_2O_5^-] \quad (8)$$

$$\text{where } [HS_2O_5^-] = K[S_2O_5^{2-}][H^+] \quad (9)$$

inserting Eqn (9) into (8);

$$\text{Rate law} = Kk_1[H^+][\text{MOC}][S_2O_5^{2-}] \quad (10)$$

$$\text{Rate law} = k[\text{MOC}][S_2O_5^{2-}] \quad (11)$$

where $k = Kk_1[H^+]$ and the rate law support the first-order actualization in the redox moieties and a single acid-dependent route. The rate law derived from the mechanism underpins first-order kinetics with respect to [MOC] and $[S_2O_5^{2-}]$ and proton assistant in the reaction, reinforcing the generated kinetic data.

Conclusions

The application of charged micelle generators on the oxidation of the metabisulphite ion by MOC uncovers a 2:1 stoichiometry and kinetics of first order in $[S_2O_5^{2-}]$ and [MOC]. The realization of sulfur dioxide product is moved by the involvement of sulfite radicals. The variation of salt concentration within the system progression incited a positive kinetic-salt-effect that describes a redox reaction stemming from like-charged molecules at the speed-limiting level of the oxidation, and the fall in the system dielectric constant retarded the rate. The catalysis initiated by the counter-ion (NH_4^+) is possible due to the involvement of negatively-charged moieties at the slow phase. The Piszkiewicz quantitative data generated exposes the great role of cationic micelles in the reaction, with a compelling binding constant that credits the impact observed in the process. The overlap of redox groups with the CTAB and SDS micelles implicated electrostatic and hydrophobic interactions as uncovered by the observed cooperativity-index. Piszkiewicz's model is appropriate in this study as it aids in informing the underlying forces of the reaction in a medium-dictated system.

Author contributions

The authors confirm contribution to the paper as follows: study conception and design: Nkole IU, Idris SO, Abdulkadir I; data collection and analysis: Onu AD, Nkole IU, Idris SO; drafted manuscript preparation, critical manuscript revision (for important intellectual content): Nkole IU, Idris SO, Abdulkadir I, Onu AD. All authors reviewed the results and approved the final version of the manuscript.

Data availability

The data from the study are available on request from the corresponding author.

Acknowledgements

Nkole I.U. is grateful to Prof. George Iloegbulam Ndukwe (former Head of Department), Department of Chemistry, Ahmadu Bello University Zaria, for his support, and the School of Science and Computing, Wigwe University Isiokpo, Nigeria.

Conflict of interest

The authors declare that they have no conflict of interest.

Dates

Received 10 February 2025; Revised 25 March 2025; Accepted 9 April 2025; Published online 15 May 2025

References

1. Trivedi HK, Patel MC. 2011. A stability indicating method for the determination of the antioxidant sodium bisulfite in pharmaceutical formulation by RP-HPLC technique. *Scientia Pharmaceutica* 79:909–20
2. Carocho M, Barreiro MF, Morales P, Ferreira ICFR. 2014. Adding molecules to food, pros and cons: a review on synthetic and natural food additives. *Comprehensive Reviews in Food Science and Food Safety* 13:377–399
3. Ahmadi F, Lee YH, Lee WH, Oh YK, Park KK, et al. 2018. Preservation of fruit and vegetable discards with sodium metabisulfite. *Journal of Environmental Management* 224:113–21
4. Vieira HH, Toledo JC Jr, Catelan A, Gouveia THN, Aguiar FHB, et al. 2018. Effect of sodium metabisulfite gel on the bond strength of dentin of bleached teeth. *European Journal of Dentistry* 12:163–70
5. D'Amore T, Di Taranto A, Berardi G, Vita V, Marchesani G, et al. 2020. Sulfites in meat: occurrence, activity, toxicity, regulation, and detection. a comprehensive review. *Comprehensive Reviews in Food Science and Food Safety* 19:2701–20
6. Carrabs G, Smaldone G, Carosielli L, Girasole M, Iammarino M, et al. 2017. Detection of sulfites in fresh meat preparation commercialised at retail in Lazio region. *Italian Journal of Food Safety* 6:93–95
7. Baker MT, Gregerson MS, Martin SM, Buettner GR. 2023. Free radical and drug oxidation products in an intensive care unit sedative: propofol with sulfite. *Critical Care Medicine* 31:787–92
8. Alimohammadi A, Moosavy MH, Amin Doustvandi M, Baradaran B, Amini M, et al. 2021. Sodium metabisulphite as a cytotoxic food additive induces apoptosis in HFFF2 cells. *Food Chemistry* 358:129910
9. Zohra EF, Yasmina BM, Samira M, Zohra SF, Soraya D, et al. 2017. Effect of sodium metabisulfite on lipid peroxidation and enzyme activities in adult rat stomach and spleen. *South Asian Journal of Experimental Biology* 7:1–8
10. Ercan S, Basaranlar G, Gungor NE, Kencebay C, Sahin P, et al. 2013. Ghrelin inhibits sodium metabisulfite induced oxidative stress and apoptosis in rat gastric mucosa. *Food and Chemical Toxicology* 56:154–61
11. Shojaee S, Nokhodchi A, Cumming I. 2014. The role of filler and sodium metabisulphite on drug release from aged polyox tablets. *Drug Development and Industrial Pharmacy* 40:1451–58
12. Alahmadi M, Alsaedi WH, Mohamed WS, Hassan HMA, Ezzeldien M, et al. 2023. Development of Bi_2O_3/$MoSe_2$ mixed nanostructures for photocatalytic degradation of methylene blue dye. *Journal of Taibah University of Science* 17:2161333
13. Sar P, Saha B. 2020. Potential application of Micellar nanoreactor for electron transfer reactions mediated by a variety of oxidants: a review. *Advances in Colloid and Interface Science* 284:102241
14. Rakshit A, Chowdhury S, Acharjee A, Mahali K, Saha R, et al. 2023. A synergistic combination of SDS and TX-100 for the catalytic oxidation of an aromatic alcohol in aqueous media. *Research on Chemical Intermediates* 49:4025–40
15. Chowdhury B, Sar P, Kumar D, Saha B. 2022. Advancement of Cu(III) and Fe(III) directed oxidative transformations: recent impact of aqueous micellar environment. *Journal of Molecular Liquids* 347:117993
16. Laguta AN, Eltsov SV, Mchedlov-Petrossyan NO. 2019. Micellar rate effects on the kinetics of nitrophenol violet anion reaction with HO^- ion: comparing Piszkiewicz's, Berezin's, and Pseudophase Ion-exchange models. *Journal of Molecular Liquids* 277:70–77
17. Nkole IU, Idris SO, Abdulkadir I, Onu AD. 2022. Effect of surfactant micellization on the oxidation of mercaptobenzothiazole by bioinorganic molybdenum complex. *Results in Chemistry* 4:100616
18. Nkole IU, Idris SO, Onu AD, Abdulkadir I. 2022. The study of Piszkiewicz's and Berezin's models on the redox reaction of allylthiourea and bis-(2-pyridinealdoximato)dioxomolybdate(IV) complex in an aqueous acidic medium. *Beni-Suef University Journal of Basic and Applied Sciences* 11:68
19. Srivastava A, Srivastava N, Tiwari D, Nayak R, Naik RM. 2024. Role of surfactants on Fe^{2+} mediated oxidative decolorization of Acid Red-13 by peroxydisulfate. *Journal of Dispersion Science and Technology*
20. Srivastava A, Dohare RK, Srivastava N, Singh R. 2025. Cu(II) mediated oxidation of L-phenylalanine with chromic acid in micellar medium: a kinetic and mechanistic approach. *Main Group Chemistry* 24:24–36
21. Srivastava A, Goswami MK, Tiwari D, Srivastava N, Srivastava K. 2023. Rate enhancement of Os(VIII) catalyzed L-phenylalanine oxidation by hexacyanoferrate(III) by CTAB micellar medium: a kinetic study. *Monatshefte Für Chemie* 154:1243–51
22. Srivastava A, Goswami MK, Singh R, Srivastava N. 2024. Os(VIII) accelerated oxidation of L-leucine by hexacyanoferrate(III) in CTAB micellar medium. *Journal of Dispersion Science and Technology* 45:2240–48
23. Srivastava A, Goswami MK, Dohare RK, Srivastava N, Srivastava K. 2023. Effect of cationic surfactant on Ru(III) catalyzed L-glutamic acid oxidation by hexacyanoferrate(III). *International Journal of Chemical Kinetics* 55:431–40
24. Srivastava A, Srivastava N, Dohare RK. 2025. Kinetic and mechanistic investigation of L-phenylalanine oxidation by alkaline Cu(III) periodate in CPC micellar medium. *Journal of Physical Organic Chemistry* 38:e4669
25. Srivastava A, Srivastava N, Srivastava K, Singh R. 2023. Rate enhancement of Cu(II) catalyzed L-glutamic acid oxidation by hexacyanoferrate (III) via micelle encapsulation. *Russian Journal of Physical Chemistry A* 97:3249–58
26. Williams RJP, Fraústo da Silva JJR. 2002. The involvement of molybdenum in life. *Biochemical and Biophysical Research Communications* 292:293–99
27. Konidaris KF, Raptopoulou CP, Psycharis V, Perlepes SP, Manessi-Zoupa EM, et al. 2010. Use of the 2-pyridinealdoxime/N,N'-donor ligand combination in cobalt(III) chemistry: synthesis and characterization of two cationic mononuclear cobalt(III) complexes. *Bioinorganic Chemistry and Applications* 7:159656
28. Arthur DE, Nkole IU, Osunkwo CR. 2021. Electron transfer reaction of tris-(1,10-phenanthroline)cobalt(III) complex and iodide ion in an aqueous acidic medium. *Chemistry Africa* 4:63–69
29. Umoru PE, Nkole IU, Ezeh TT. 2024. Degradation of indigo carmine dye with peroxydisulphate ion in aqueous sulphuric acid phase: kinetic study. *International Journal of Chemical Kinetics* 56:339
30. Nkole IU, Idris SO, Abdulkadir I, Onu AD. 2024. Oxidation of aspartic acid with molybdenum-oxime-ligand framework in acidified-aqua and interfacial active media: Menger-Portnoy kinetic model. *Inorganic Chemistry Communications* 161:111979
31. Adetoro A, Idris SO, Onu AD, Okibe FG. 2018. Electron transfer reaction of glutamic acid and synthesized bis-(ethylenediamine)succinimidatocobalt(III) dinitrate dihydrate in aqueous hydrochloric acid medium. *FUW Trend in Science and Technology Journal* 3:246–251
32. Dennis CR, Van Zyl GJ, Fourie E, Basson SS, Swarts JC. 2021. A kinetic study of the oxidation of the tetrakisoxalatouranate(IV) ion by the hexacyanoferrate(III) ion in an oxalate buffer medium. *Reaction Kinetics, Mechanisms and Catalysis* 132:599–615
33. Idris SO, Suleiman JO, Iyun JF, Osunlaja AA. 2015. Reduction of 3,7-bis(dimethylamino)phenazothionium chloride by benzenethiol in aqueous nitric acid medium: a mechanistic approach. *American Chemical Societal Journal* 5:313–21
34. Kumagai Y, Barreiro Fidalgo A, Jonsson M. 2019. Impact of stoichiometry on the mechanism and kinetics of oxidative dissolution of UO_2 induced by H_2O_2 and γ-irradiation. *The Journal of Physical Chemistry C* 123:9919–25
35. Osunkwo CR, Nkole IU, Onu AD, Idris SO. 2018. Electron transfer reaction of tris-(1,10-phenanthroline)cobalt(III) complex $[Co(phen)_3]^{3+}$ and thiosulphate ion ($S_2O_3^{2-}$) in an aqueous acidic medium. *International Journal of Advance Chemistry* 6:121–26
36. Nkole IU, Idris SO, Abdulkadir I, Onu AD. 2023. Cationic surfactant-based catalysis on the oxidation of glutamic acid by bis-(2-pyridinealdoximato)dioxomolydate(IV) complex. *Catalysis Letters* 153:3581–90

37. Onu AD, Iyun JF, Idris SO. 2015. Kinetics and stoichiometry of the reduction of hydrogen peroxide by an aminocarboxylactocobaltate(II) complex in aqueous medium. *Open Journal of Inorganic Chemistry* 5:75–82
38. Lakk-Bogáth D, Kripli B, Meena BI, Speier G, Kaizer J. 2019. Catalytic and stoichiometric CH oxidation of benzylalcohols and hydrocarbons mediated by nonheme oxoiron(IV) complex with chiral tetrapyridyl ligand. *Inorganic Chemistry Communications* 104:165–170
39. Asghar BH, Fawzy A. 2016. Kinetic, mechanistic, and spectroscopic studies of permanganate oxidation of azinylformamidines in acidic medium, with autocatalytic behavior of manganese(II). *Journal of Saudi Chemical Society* 20:561–569
40. Fawzy A. 2016. Kinetic and mechanistic aspects of oxidation of aminotriazole formamidine by cerium(IV) in aqueous perchloric and sulfuric acid solutions: a comparative study. *Journal of Solution Chemistry* 45:246–64
41. Tekle-Röttering A, von Sonntag C, Reisz E, Vom Eyser C, Lutze HV, et al. 2016. Ozonation of anilines: kinetics, stoichiometry, product identification and elucidation of pathways. *Water Research* 98:147–59
42. Fawzy A, Fawzi A. 2023. Oxidative degradation of sulfafurazole drug by chromium trioxide in different acidic media: a kinetic and mechanism study. *Journal of Umm Al-Qura University for Applied Sciences* 9:276–84
43. Valdebenito A, Encinas MV. 2010. Effect of solvent on the free radical polymerization of N, N-dimethylacrylamide. *Polymer international* 59:1246–51
44. Osunkwo CR, Nkole IU, Onu AD, Idris SO. 2018. Kinetics and mechanism of the reduction of tris-(1,10-phenanthroline)cobalt(III) complex by n-methylthiourea in aqueous acidic medium. *Nigerian Research Journal of Chemical Sciences* 5:82–93
45. Nkole IU, Idris SO, Abdulkadir I, Onu AD. 2022. Application of Piszkiewicz model on the electron transfer reaction of dithionite ion and bis-(2-pyridinealdoximato)dioxomolybdate(IV) complex. *Scientific Reports* 12:22125
46. De Sterck B, Vaneerdeweg R, Du Prez F, Waroquier M, Van Speybroeck V. 2010. Solvent effects on free radical polymerization reactions: the influence of water on the propagation rate of acrylamide and methacrylamide. *Macromolecules* 43:827–36
47. Ibrahim I, Idris SO, Abdulkadir I, Onu DA. 2022. Thioglycolic acid oxidation by N,N'-phenylenebis(salicylideneiminato)manganese(III) in DMSO/H_2O: effects of sodium dodecylsulfate and cetyltrimethylammonium bromide. *Results in Chemistry* 4:100541
48. Laguta AN, Eltsov SV, Mchedlov-Petrossyan NO. 2019. Kinetics of alkaline fading of methyl violet in micellar solutions of surfactants: comparing Piszkiewicz's, Berezin's, and Pseudophase Ion-exchange models. *International Journal of Chemical Kinetics* 51:83–94
49. Dahadha AA, Abunuwar M, Al-qderat M, Al-Abrouni KF. 2023. N-dodecyl β-D-glucopyranoside micelles catalyzed reaction of ascorbic acid with azure A chloride salt dye in acidic aqueous solution: A kinetic, thermodynamic and mechanism study. *Colloid and Polymer Science* 302:333–343
50. Subramaniam P, Vanitha T, Kodispathi T, Sundari CRS. 2014. Role of iron(III)-salen chloride as oxidising agent with thiodiglycolic acid: the effect of axial ligands. *Journal Mexican Chemical Society* 58:211–17
51. Pizzolato E, Natali M, Posocco B, Montellano López A, Bazzan I, et al. 2013. Light driven water oxidation by a single site cobalt salophen catalyst. *Chemical Communications* 49:9941–43
52. Ibrahim I, Idris SO, Abdulkadir I, Onu AD. 2019. Kinetics and mechanism of the redox reaction of *N,N'*-phenylenebis-(salicylideneiminato)iron(III) with oxalic acid in mixed aqueous medium. *Transition Metal Chemistry* 44:269–73
53. Ngan NK, Lo KM, Wong CSR. 2012. Dinuclear and polynuclear dioxomolybdenum(VI) schiff base complexes: synthesis, structural elucidation, spectroscopic characterization, electrochemistry and catalytic property. *Polyhedron* 33:235–51
54. Abdulsalam S, Idris SO. 2016. Kinetics and mechanism of redox reaction of crystal violet and metabisulphite ion in aqueous acidic medium. *Gashua Journal of Sciences and Humanities* 2:19–26
55. Maila MD, Maree JP, Cele LM. 2014. Acid mine water neutralisation with ammonium hydroxide and desalination with barium hydroxide. *Water SA* 40:521–28
56. Jeffery GH, Bassett J, Mendham J, Denney RC. 1989. *Vogel's textbook of quantitative chemical analysis*. 5th Edition. UK: Longman Scientific & Technical. xxix+877 pp.
57. Khraibah NH. 2010. Kinetics of the reduction of hexacyanoferrate(III) with metabisulfite as function of pH. *Journal of King Abdulaziz University-Science* 22:65–76
58. Jiang BY, Du J, Cheng SQ, Wang Q, Zeng XC. 2003. Effects of amine additives on critical micelle concentration of ionic surfactants. *Journal of Dispersion Science and Technology* 24:755–60
59. Li W, Zhang M, Zhang J, Han Y. 2006. Self-assembly of cetyltrimethylammonium bromide in ethanol-water mixtures. *Frontiers of Chemistry in China* 1:438–42